AFRL-AFOSR-JP-TR-2022-0009

CNT Network (Web) and Wall (Curtain) Structures

Lee, Haiwon
HANYANG INDUSTRY-UNIVERSITY COOPERATION
HAENGDANG 1DONG, SEONGDONG-GU, SEOULRM110. HIT, HANYANG UNIV. 17
SEOUL, ,
KR

12/03/2021
Final Technical Report

Air Force Research Laboratory
Air Force Office of Scientific Research
Asian Office of Aerospace Research and Development
Unit 45002, APO AP 96338-5002

REPORT DOCUMENTATION PAGE

Form Approved
OMB No. 0704-0188

1. REPORT DATE *(DD-MM-YYYY)*	**2. REPORT TYPE**	**3. DATES COVERED** *(From - To)*
03-12-2021	Final	30 Sep 2017 - 29 Sep 2020

4. TITLE AND SUBTITLE
CNT Network (Web) and Wall (Curtain) Structures

5a. CONTRACT NUMBER
FA2386-17-1-4080

5b. GRANT NUMBER

5c. PROGRAM ELEMENT NUMBER
61102F

6. AUTHOR(S)
Haiwon Lee

5d. PROJECT NUMBER

5e. TASK NUMBER

5f. WORK UNIT NUMBER

7. PERFORMING ORGANIZATION NAME(S) AND ADDRESS(ES)
HANYANG INDUSTRY-UNIVERSITY COOPERATION
HAENGDANG 1DONG, SEONGDONG-GU, SEOULRM110. HIT, HANYANG UNIV. 17
SEOUL,
KR

8. PERFORMING ORGANIZATION REPORT NUMBER

9. SPONSORING/MONITORING AGENCY NAME(S) AND ADDRESS(ES)
AOARD
UNIT 45002
APO AP 96338-5002

10. SPONSOR/MONITOR'S ACRONYM(S)
AFRL/AFOSR IOA

11. SPONSOR/MONITOR'S REPORT NUMBER(S)
AFRL-AFOSR-JP-TR-2022-0009

12. DISTRIBUTION/AVAILABILITY STATEMENT
A Distribution Unlimited: PB Public Release

13. SUPPLEMENTARY NOTES

14. ABSTRACT
The report was received quite late.

15. SUBJECT TERMS

16. SECURITY CLASSIFICATION OF:			**17. LIMITATION OF ABSTRACT**	**18. NUMBER OF PAGES**	**19a. NAME OF RESPONSIBLE PERSON**
a. REPORT	**b. ABSTRACT**	**c. THIS PAGE**			JEREMY KNOPP
U	U	U	SAR	14	**19b. TELEPHONE NUMBER** *(Include area code)* 315-227-7006

Hierarchical Nanostructured Materials Based on Carbon Nanotubes for Battery Electrodes

Name of Principal Investigator: Haiwon Lee

- e-mail address: haiwon@hanyang.ac.kr
- Institution: Hanyang University
- Mailing. address: Department of Chemistry, Hanyang University, 222 Wangshimni-ro, Seongdong-gu, Seoul 04763, Korea
- Phone: +82-2-2220-1934
- Fax: +82-2-2220-1935

Period of Performance: 30/09/2017 – 29/09/2020

Summary

The objective of the project was to investigate a noble nanostructured architecture based on CNTs for the electrodes in both Li-S battery and fuel cell when the proposal was accepted. The synthesis of CNTs, design and fabrication of hierarchical nanostructures, surface modification, sulfur and platinum loading, and characterization and performance of designed electrodes were proposed to be carried out. However, the scope of proposed research was revised in the second year since the proposed nanostructured architecture was not very challenging to continue to investigate a candidate electrode for both hydrogen fuel cell and Li-S battery system. Instead of investigating the performance of our designed electrode structure continuously the PI changed the directions of proposed research by focusing on the basic study of noble anode current collector for Li-S battery and the self-assembly approach to deposit the Pt particles uniformly onto the functionalized CNTs grown on Si substrates. The CNT grown on Si and Cu substrates by using thermal CVD and surface functionalization was used as a capping material with its high electrical conductivity and superior chemical stability for the basic study of nanostructured materials as a component in Li-S battery and hydrogen fuel cell. The adsorption of Pt nanoparticles on N-terminated CNTs on Si substrate

in a solution process was well carried out and the effect of CNTs in-situ grown Cu nanowire porous current collector in accommodating lithium for the improvement of lithium anode performance was investigated.

[Accommodating Lithium into a CNT in-situ Grown Cu Nanowire Porous Current Collector for Improving Lithium Anode Performance]

Introduction

Current collector is a key component bridging lithium-ion batteries and external circuits, greatly influencing the capacity, rate capability and long-term stability of lithium-ion batteries. Conventional current collectors of Al and Cu foils have been used for the last two decade, and nanostructured Cu foil formed by specific treatments such as etching and carbon coating have been investigated to enhance the electrochemical stability and electrical conductivity of current collectors. Lithium metal has been well used as an ideal anode material in lithium batteries. However, the problems of dendritic and mossy Li formation hindered the practical application of Li metal anode in past four decades. The formation of dendritic Li during Li plating would lead to low Coulombic efficiency, short cycle life, internal short circuits and even catastrophic cell failure. As a key component of the anode, the current collector could also have a significant influence on the Li anode. The current collector affects the nucleation at the initial period of Li plating, which is decisive for the morphology of the subsequently plated Li. A three-dimensional (3D) current collector with a submicron-sized skeleton and porous structure can change the plating behavior. When the porous Cu foil is used as the 3D current collector, Li grows on the submicron-sized Cu skeleton and fills the pores of the 3D current collector. An interfacial layer with a lithiophilic-lithiophobic gradient was reported to provide better control of Li deposition and suppress dendrite growth. Current collector can guide bottom-to-top Li nucleation/deposition and suppress Li dendrites. In this report, a functionalized CNT in-situ grown 3D porous Cu nanowire (f-CNT/CuNW/Cu) template is used as the anode current collector which can change the lithium plating behavior and improving the Li anode performance. When the porous f-CNT/CuNW/Cu is used as the 3D current collector, lithium grows on the NH_3 modified CNT surface using plasma treatment and fills the nano-sizde pores constructed by the Cu nanowire skeleton and CNTs. Li metal is stably sustained by the CNT layer and CuNW skeleton. Together with the top side lithiophobic C_2H_2 plasma polymerized layer, this gradient interfacial layer can effectively suppress dendrite growth and ensure ultralong-term stable lithium stripping/ plating. With Li-metal anode accommodated in the 3D current collector, we can get Li metal anodes free from the Li dendrite crux and improve the lifespan of Li-metal anodes.

Basic Concepts of Proposed Nanostructures for Electrodes:

- **Fuel Cell**

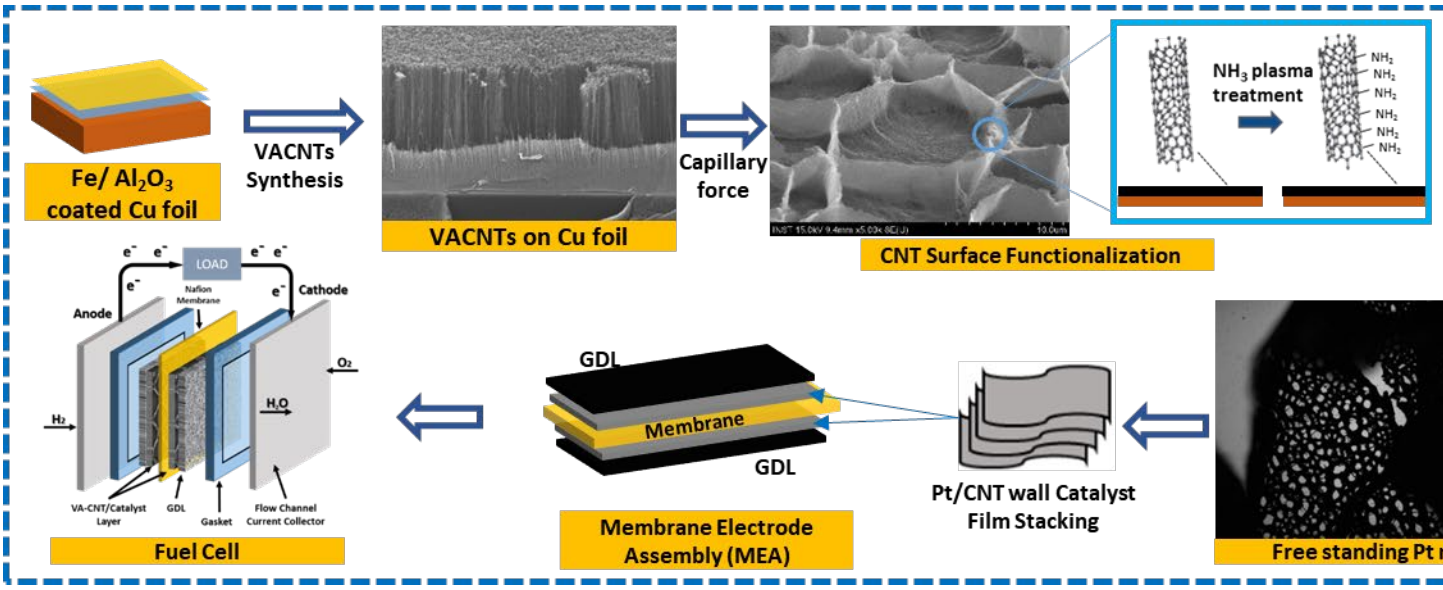

■ **Li-S Battery Electrode**

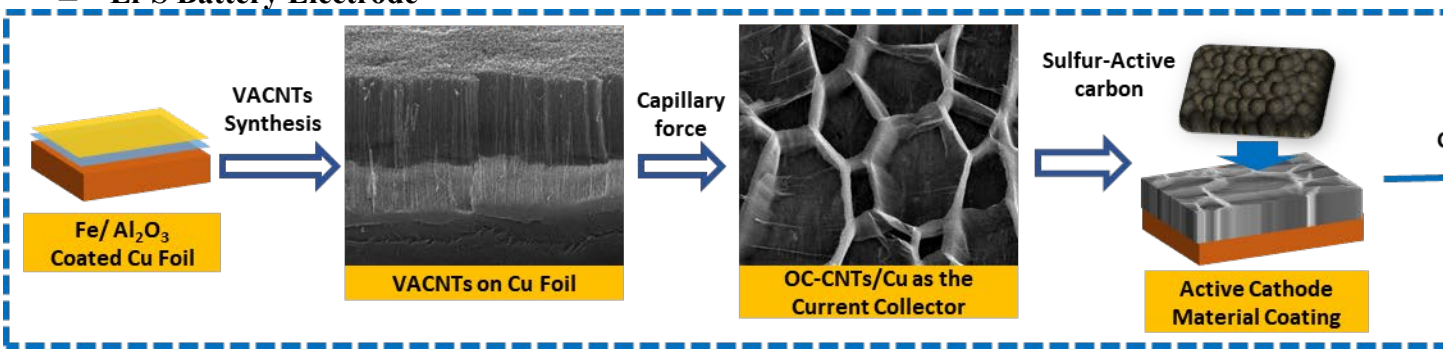

Scheme of a New Nanostructure for Current Collector

■ **Li-S Battery Current Collector**

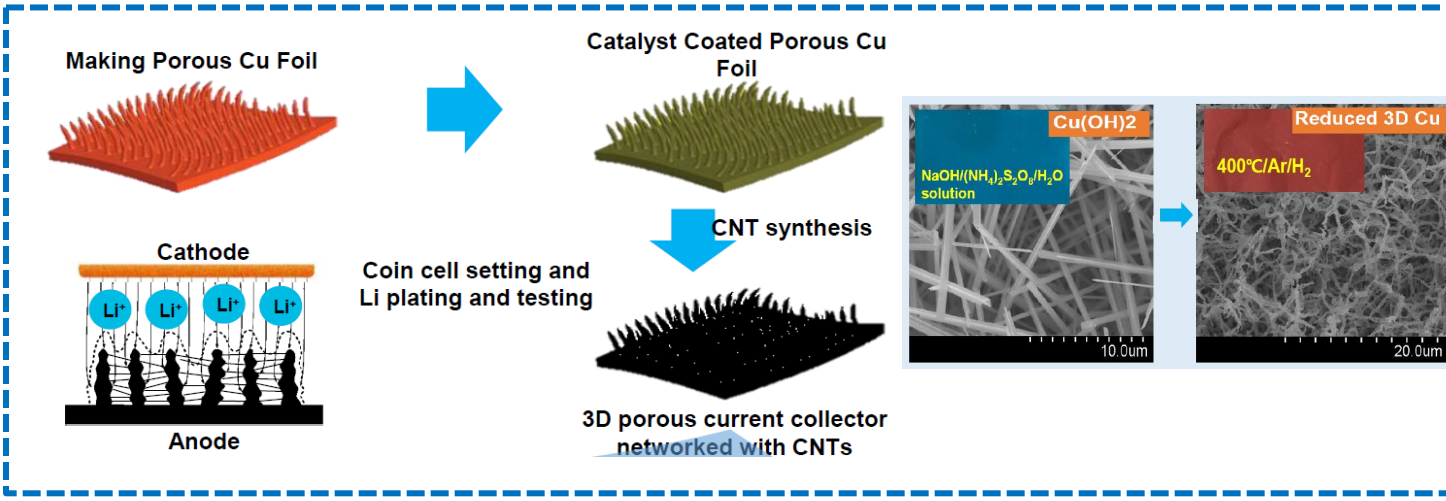

Results and Discussions

Synthesis of Cu nanowires

The 3D porous Cu foil is fabricated from a commercial planar Cu foil via a facial and scalable method which has been widely used and reported in elsewhere. The method involves etching of copper from the foil surface and redeposition as copper hydroxide or copper oxide nanostructures. A subsequent heat treatment step in hydrogen reduced the $Cu(OH)_2$ into Cu nanowire arrays, with retention of the original nanostructure as shown in Figure 1. Different variations of the nanowire growth process produced either copper hydroxide or copper oxide nanostructures. By fine-tuning the growth conditions, different morphologies of the nanoscale features were realized. These morphologies include nanowires, nanoribbons, and nanotubes. The original copper hydroxide or copper oxide nanostructures formed were phase pure single crystals, which were converted into polycrystalline copper by the reduction process. The primary process developed in this study comprises three steps: (i) surface cleaning via sonication to remove any adhered impurities (and to introduce atomic-scale defects); (ii) nanowire growth using an etching solution of sodium hydroxide and APS; and (iii) gas-phase reduction through heating in hydrogen. When copper surfaces are exposed to an alkaline oxidant solution, a blue film of $Cu(OH)_2$ gradually grows on the copper surface. The nanostructure growth process and shape are very much dependent on the growth conditions, including temperature, concentration of solutes and time of exposure to the alkaline oxidant solution. Structural analysis of the as-obtained $Cu(OH)_2$ nanowires was performed by XRD, and the result is displayed in Figure 1d. All the diffraction peaks of the $Cu(OH)_2$ can be assigned to orthorhombic symmetry of CH (JCPDF 35–0505). Besides the three peaks of 43.4°, 50.6° and 74.5° attributed to (111), (200) and (220) plane are indexed to cubic Cu (JCPDF 65–9743) of the substrate. No peaks of impurities were found, indicating the high purity of the as-prepared $Cu(OH)_2$. The as-obtained $Cu(OH)_2$ nanowires were heated at 120 ℃for 2 hrs for dehydration and reduced at 400 ℃ for 10 h in a H_2/Ar mixed flow (5% H_2 in volume) to get the 3D porous Cu foil. Based on the differences in density, the reduction of copper hydroxide nanowires to copper nanowires would be expected to produce a 75% decrease in volume. A significant decrease in nanowire diameter and no apparent change in length is observed. The final Cu foil shows a 3D structure composed of bundles of Cu fibers, as shown in the SEM images (Fig. 1b) The Cu fibers are several submicron in diameter and have a nanosized protuberant secondary structure on the surface, as shown in the inset in Fig. 1b. After reduction of the nanowires the disappearance of the peaks at 23.6°, 33.9°, 35.9°, 38.1°, 39.6° and 53.2° positions is consistent with the conversion of copper hydroxide to metallic copper.

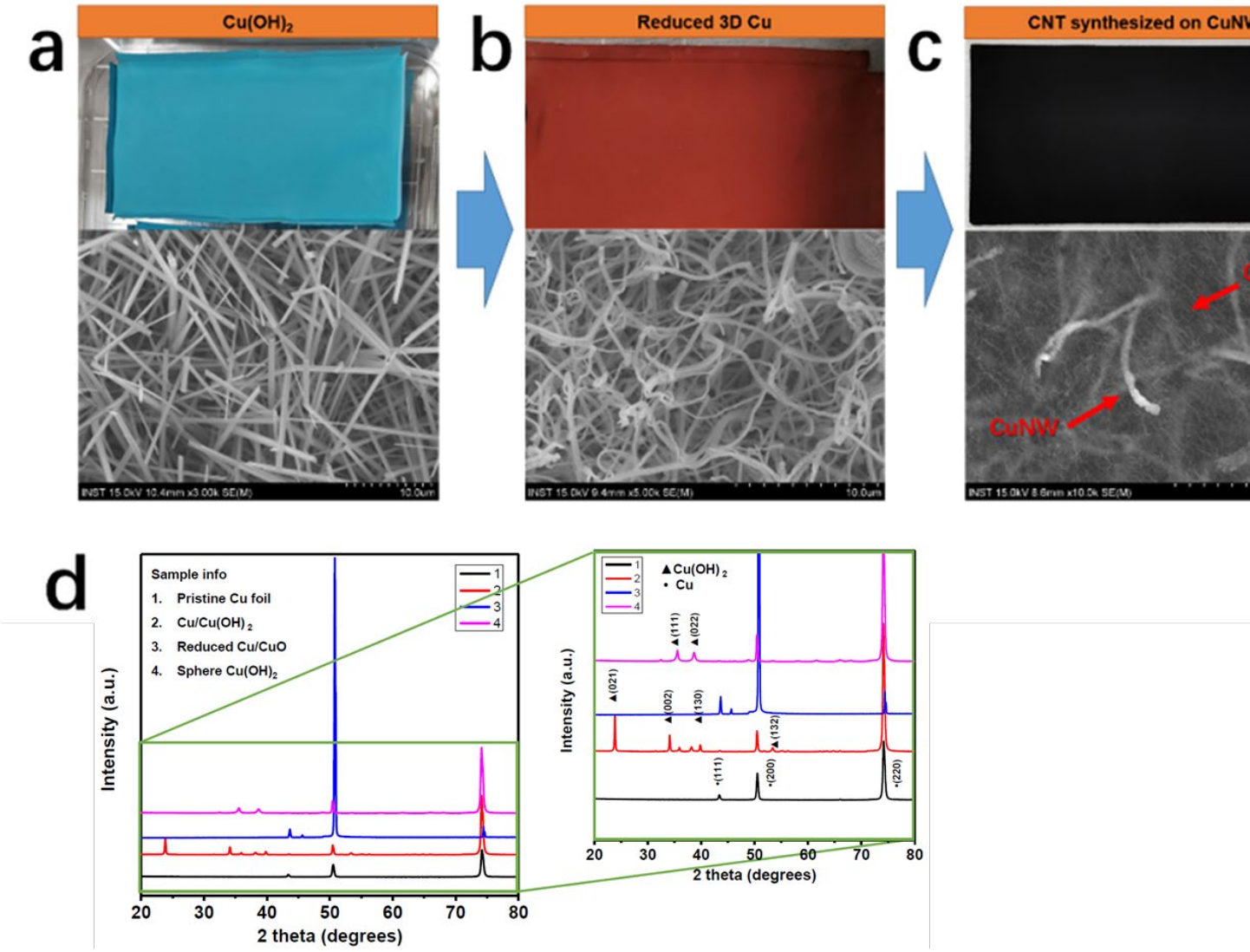

Figure 1. SEM images of synthesized a) $Cu(OH)_2$ nanowires, b) reduced Cu nanowires, and c) CNTs grown on the reduced Cu nanowires; d) XRD of pristine Cu foil, $Cu(OH)_2$ nanowires and reduced Cu nanowires.

CNT growth on Cu nanowires

The reduced CuNW foil is coated with Al_2O_3 (10nm) and Fe (10nm) by ALD and E-beam deposition, respectively. The synthesis was carried out by a Thermal CVD with a horizontal quartz tube furnace with an inner diameter of 2 inch. Firstly, Ar (500 sccm) was used as a carrier gas to deliver the decomposition gas to the furnace. Ar was also used to purge for 30 min while the tube furnace was ramped up to 700°C. After reaching at 750°C, H_2 (200 sccm) was supplied as reduction gas and Ar (500 sccm) gas was supplied as carrier gas for 10 min. The gas flow was then switched to C_2H_2 (30 sccm), Ar (500 sccm) and H_2 (200 sccm) for 1 hr for the CNT growth. The CNTs were cooled down to ambient temperature after completion of the reaction. A porous layer of CNTs are successfully synthesized in between the CuNWs as shown in Figure 1c. Depending on the Raman

spectroscopy (Figure 1e) and TEM image (Figure 1f), the as-synthesized CNTs are multiwalled CNTs with an average diameter of ~10nm.

Plasma functionalization of CNT/CuNW/Cu

CNT/CuNW/Cu were treated with NH_3 (30 sccm) plasma at 50 W, 0.11 torr, ambient temperature using PECVD for 20 min to confirm the amino groups. The surface was modified without any morphology deformation. After NH_3 plasma treatment, C_2H_2 plasma treatment is carried out in the condition of 0.05 torr and 50 W at room temperature for 3 min. After the plasma treatment, reactive gas was removed by the vacuum state for 5 min on pressure less than ca. 5.0 x 10-6 torr. The surface chemical compositions of the pristine CNTs and NH_3/ C_2H_2 plasma-treated CNTs were determined by the XPS spectra. Figure 2 shows the XPS spectra of pristine CNTs and after plasma treatment. Figure 2d shows the content of C, O, and N of pristine and plasma-treated CNTs. The pristine 3D network of CNTs have about 98.69 at. % of carbon and 1.32 at. % of oxygen. The oxygen might come from ambient air contamination. After NH_3 plasma treatment, the nitrogen atoms were obviously detected on the surface as shown in Figure 2b, d. After C_2H_2 plasma treatment, at. % of carbon is decreased to 94.47% and at. % of oxygen is slightly enhanced to 5.53% on the C_2H_2 plasma-treated surface.

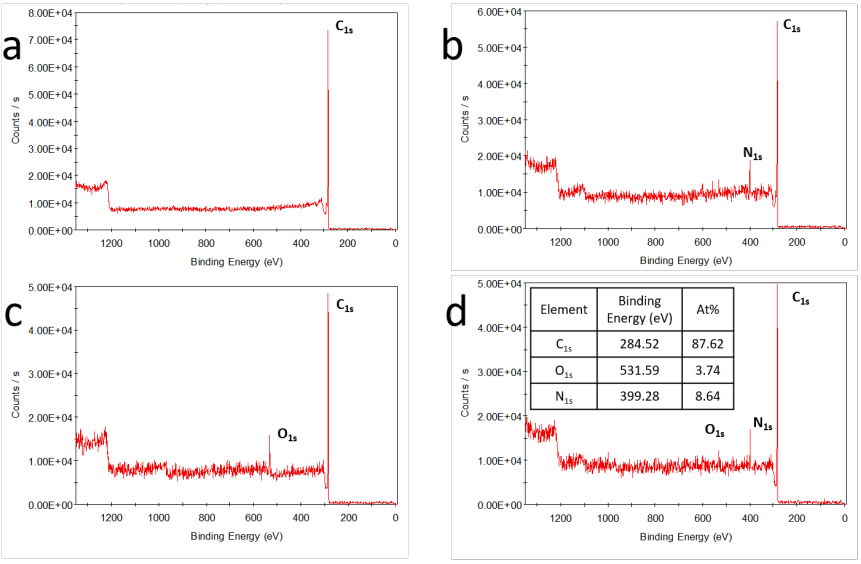

Figure 2. XPS spectra of (a) pristine CNTs, (b) NH_3 plasma-treated CNTs (c) C_2H_2 plasma-treated CNTs and (d) NH_3/ C_2H_2 plasma-treated CNTs; inset of (d) is the table of atomic concentration of C, O, and N.

Li-metal deposition behavior

The f-CNT/CuNW/Cu was utilized to investigate the plating behaviour of Li metal on a 3D current collector. The pristine Cu foil was also tested as an example of planar current collectors. On a planar current collector, Li is apt to firstly form small Li dendrites on the smooth surface at the nucleation step. The subsequent Li metal is then deposited on these small Li dendrites and amplify the growth of the Li dendrites. In contrast, on the f-CNT/CuNW/Cu foil, numerous protuberant tips on the submicron fibers function as the charge centers and nucleation sites. The electric field is roughly uniform, and the charges are relatively homogeneously dispersed along the CNT

skeleton. Therefore, Li is expected to nucleate and grow on the submicron Cu fibers with nanosized lumps, fill the pores of the 3D current collector, and eventually form a relatively even Li surface.

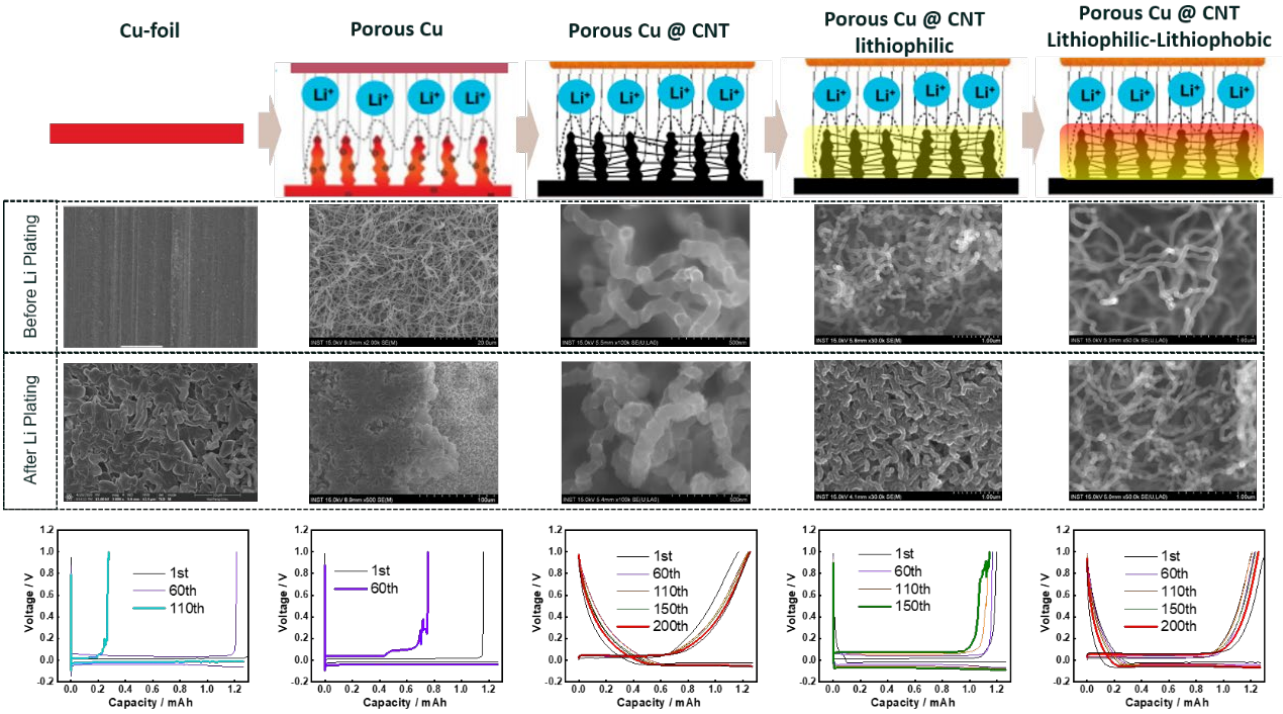

Figure 3. SEM images of Li-Cu, Li-CuNW, Li-CNT/CuNW, and Li-f-CNT/CuNW before and after Li plating. The bottom row is the asymmetric cell test of those samples.

From our initial expectation, it was expected that the charging platform of the f-CNT/CuNW/Cu sample could be the lowest compared with other samples, with the long cycles and the smallest overpotential change, so as to prove that the multilayered structure has the promotion effect on the Li ion embedding/stripping process and the inhibition effect on the dendrite. However, in Figure 3, it seems that pristine Cu foil/lithium sample has the lowest overpotential. The overpotential of 5 samples does not form a regular pattern and the results did not support our idea. The Li-CNT/CuNW sample showed that after the addition of CNT, the battery system impedance increased, which was inconsistent with the idea. The discharge capacity of the first two samples is larger than the charging capacity. In the case of Cu foil only, this phenomenon is unreasonable.

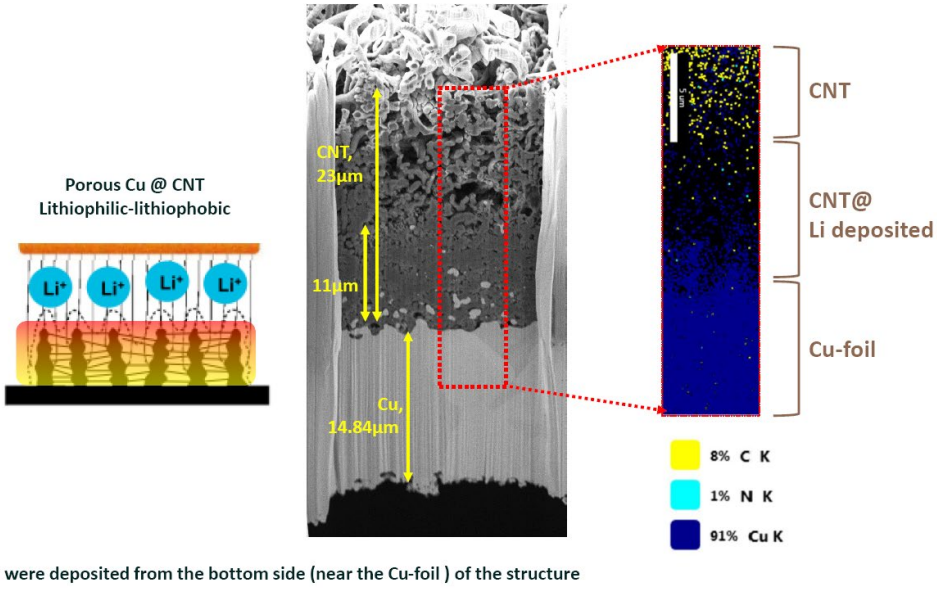

Figure 4. FIB SEM image of Li-f-CNT/CuNW.

Figure 4 shows the FIB cross section SEM image of the Li deposited f-CNT/CuNW/Cu. Li metal were mainly deposited on the bottom part of porous CuNW and CNT surfaces which means that Li ions penetrated the upper layer of lithiophobic CNT layer and accumulated to the down layer of lithiophilic CNT and CuNW layer. So, this multilayered structure realized the expected guided deposition of Li metal well.

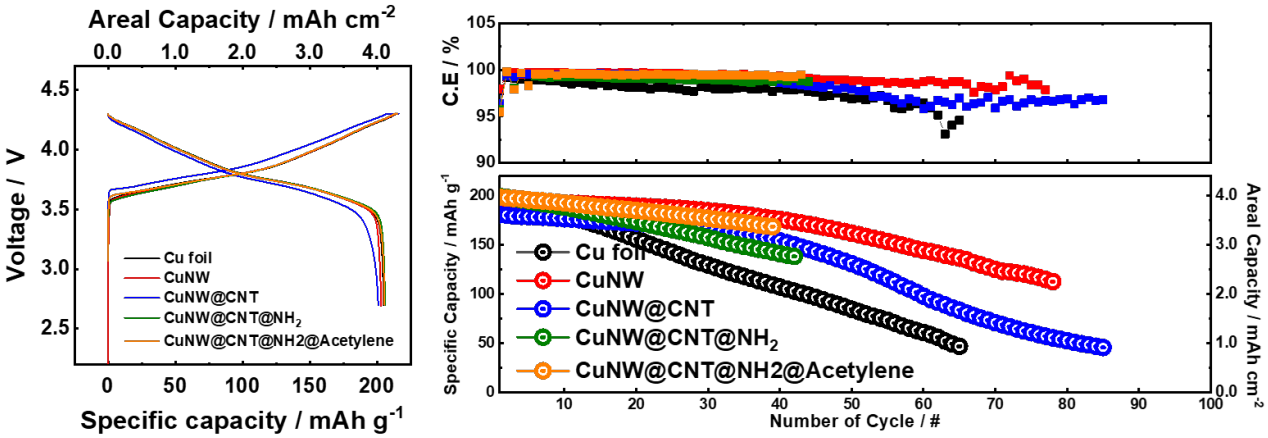

Figure 5. Full cell test.

In Figure 5, on the left side, what we expected is that the yellow charge curve should be the lowest, while the discharge curve should be the highest and have the maximum capacity. However, the current data is that the green data seems to perform the best. On the top right in the figure, the yellow Coulomb is the most efficient, which is in line with our initial idea. The order of coulomb efficiency from highest to lowest should be: black< red< blue< green< yellow. However, the current data regularity is not strong. In the figure, the volume tendency and the coulombic efficiency tendency should be the same. However, the obtained data are not consistent.

Conclusion

We successfully controlled the synthesis conditions and fabricated the f-CNT/CuNW/Cu templated as the 3D current collector for Li-metal anode. With the multilayered lithiophilic and lithiophobic design, guided Li deposition was realized which effectively suppress dendrite growth and sustained high coulombic efficiency during the lifecycle test. However, during the electrochemistry test, their charge/discharge and lifecycle tendency do not match our expectation. Sampling control and more detailed tests should be done later.

[Adsorption of Platinum Nanoparticles on Hierarchically Entangled CNT Nanostructures]

Introduction

The CNTs can be transformed into complex 3D micro-structures via an elastocapillary self-assembly process, and the mechanical deformation including the change in the arrangement of CNT bundles occurs during wetting or drying processes. If the surface forces between the contacting CNTs are stronger than capillary forces, the aggregated configuration can be stable after the liquid evaporation. If capillary forces are stronger than the elastic restoring forces for the vertically grown CNTs (V-CNTs), the CNTs are aggregated and encounter with one another. This aggregated CNT nanostructure on a substate can used as a template with high surface area in various fields once the functionalization of CNTs is well controlled. Nitrogen functionalized CNT have shown great potential for realizing increased oxidation-reduction reaction (ORR) activity, higher power density and improved long-term cycling durability by minimizing both carbon corrosion and Pt dissolution in fuel cell. This suggests that the high degree of N-surface functionalization is beneficial for carbon stability. N-doping or amine functionalization suggests a positive impact on minimizing Pt dissolution. Nitrogen is more electronegative than carbon, and consequently electron density is transferred from the adjacent C atoms to the N atoms, allowing for stronger anchoring of Pt nanoparticles. In this regard, we carefully control the adsorption process of Pt nanoparticles uniformly onto the N-terminated CNTs grown on Si substates as well as carbon fabric. The purpose of Pt nanoparticles adsorption on the surface of CNT assembly is to find the best conditions for the electrode fabrication of proton exchange membrane (PEM) fuel cell.

Adsorption of platinum nanoparticles on carbon nanotubes

Hexachloroplatinic acid hexahydrate ($H_2PtCl_6 \cdot H_2O$) was used as a precursor for the source of platinum ions and sodium borohydride ($NaBH_4$) was used as a reducing agent.

Results and Discussion

Characterization of V-CNT and H-CNT Structures

The surface morphology of vertically grown CNTs (V-CNTs) resulted from capillary forming was analyzed by using SEM. V-CNTs were synthesized by using LP- TCVD and was directly immersed in the acetone to form the aggregated CNT structure. The acetone wetted the CNTs independently within each CNT microstructure due to capillary action. Furthermore, acetone was evaporated to initiate capillary densification of CNTs. The aggregated CNTs formed by the capillary driven force self-assembly displayed honeycomb-like patterns (H-CNTs) which have a width around 5-30 μm as shown in Figure 6. As depicted in Figure 6a and 6c, H-CNT structures have a lower height (5 μm) compared to the as-grown V-CNT (24 μm) due to shrinking CNT during the capillary self-assembly process. The formed H-CNT structure also has bundle shape with an average diameter of 23 nm, and it is two time larger than the as-grown V-CNT as shown in Figure 23b and 23d. The bundle formation on H-CNT structure could be caused by van der Walls forces between CNT. However, the pattern of H-CNT was uncontrollable and tricky due to a complicated forces mechanism, therefore, the resulting structures showed irregular patterns formation.

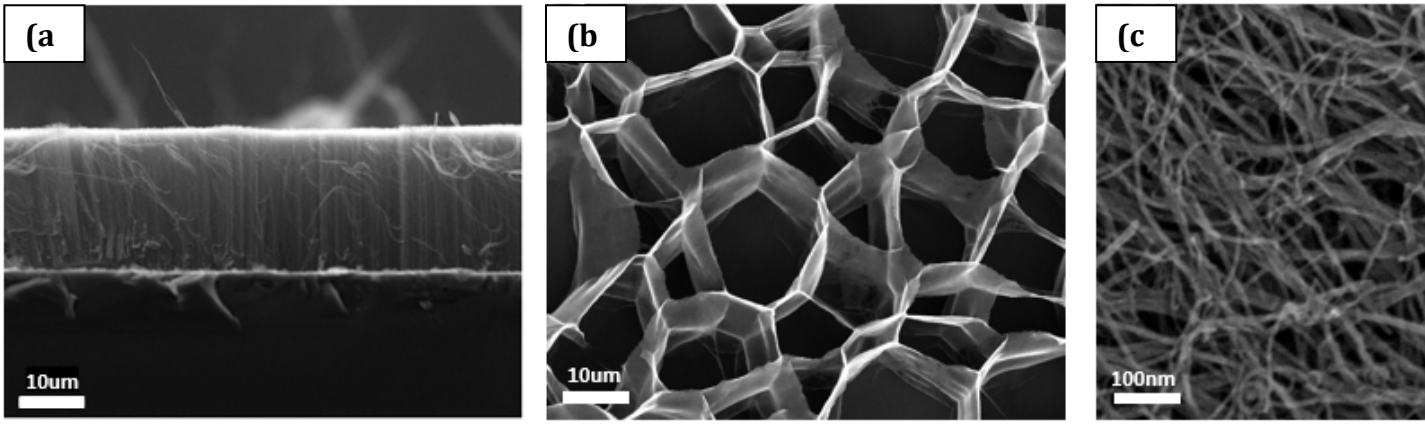

Figure 6. The V-CNTs which synthesized by LP-TCVD and acetone treated V-CNTs structures. (a) is V-CNTs height. (b) is acetone treated H-CNTs which formed using V-CNTs. (c) is corresponding high-resolution image diameter of H-CNTs is around 10-30nm.

Characterization of Pt/H-CNTs

The Pt nanoparticles which were adsorbed on the surface of the NH_3 plasma treated V-CNTs were characterized by SEM, EDS, XRD and XPS. The conditions of Pt precursor concentration and the $NaBH_4$ solution concentration were 0.05M and 0.10M, respectively. And the solvents of each solution were ethanol and mixed ethanol and DI water (9:1, v/v). As shown in Figure 7, the adsorbed Pt particles were measured by SEM. The EDS mapping results showed the dispersed Pt particles on the surface of the H-CNTs as shown in Figure 8. The Pt particles were dispersed well on the surface of CNTs. And the results of XRD analysis of the synthesized Pt nanoparticles are shown in Figure 9. The structures of all samples were H-CNTs. And 1, 2, 3-Pt/CNTs samples were prepared by repeated adsorption process under the same conditions (0.05M Pt solution,0.10M

NaBH4). In Figure 11, the same peak appears in all samples at around 25° is due to the C (200) which come from the CNTs as the supporter. The characteristic diffraction peaks of Pt(111), Pt(200), Pt(220) and Pt(311) were observed at 2θ values of 39.9°, 46.2°, 67.9° and 82.4° as shown in the ICSD database of Pt number 64923. This indicates that Pt nanoparticles were successfully reduced and had a face-centered cubic (fcc) phase structures. The average size of reduced Pt particles (d) from each sample were calculated by Scherrer equation.

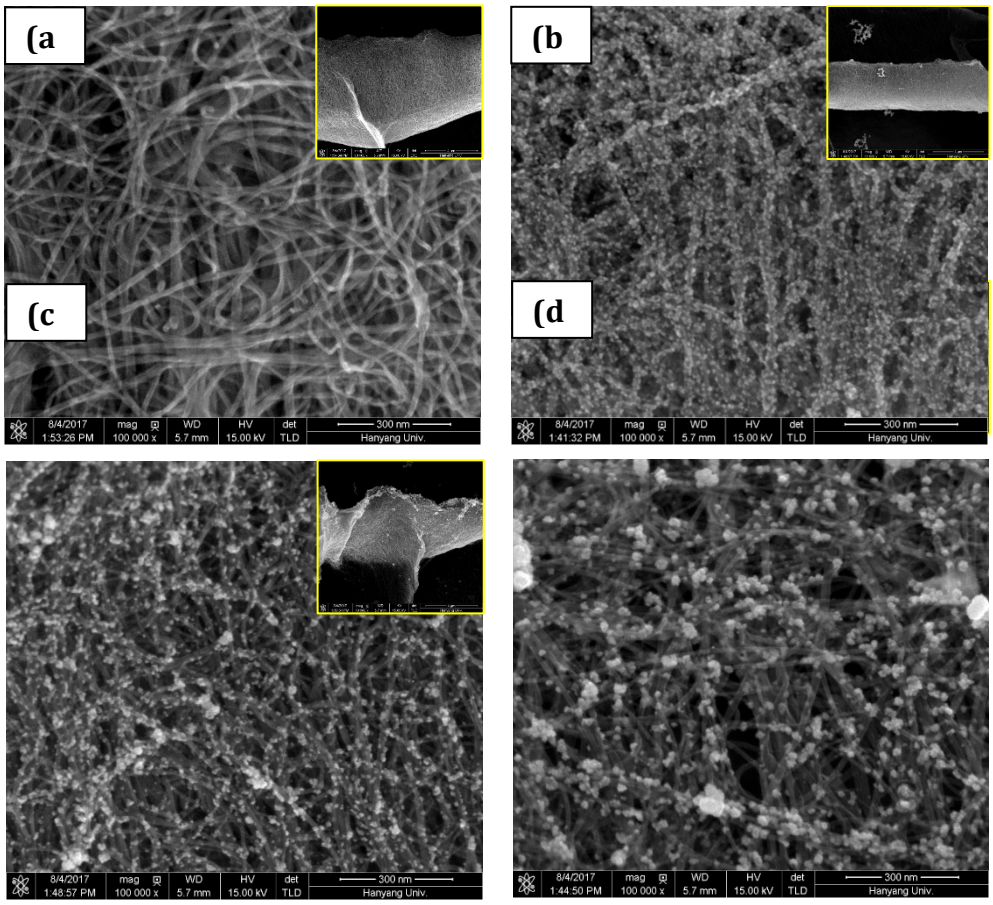

Figure 7. SEM images of Pt nanoparticles on the surface of CNTs. The all concentration of H_2PtCl_6 was 0.05M for (a). (a) is bare CNTs which have no Pt particles. (b) was adsorbed Pt nanoparticles under 0.10M NaBH4 so (c) was adsorbed under 0.25M, and (d) was adsorbed under 0.50M.

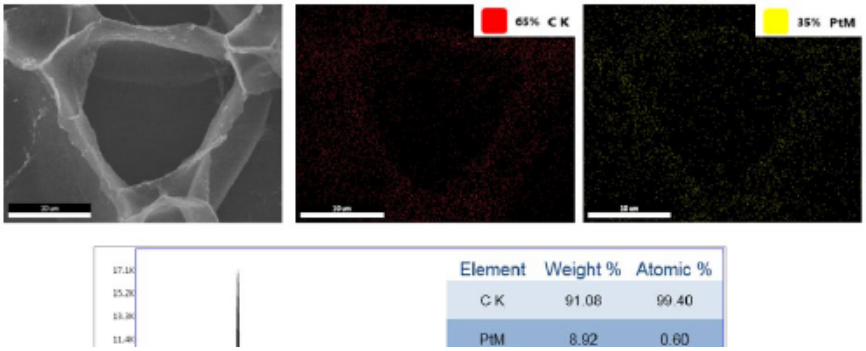

Figure 8. (a) is the EDS mapping patterns of the Pt nanoparticles for a wider area and (b)the elemental analysi
Pt.

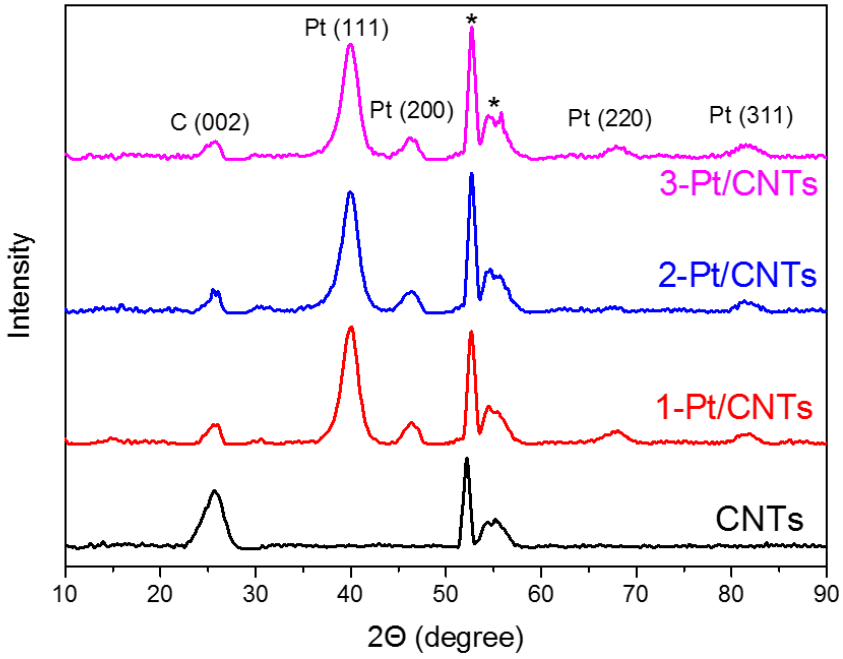

Figure 9. X-ray diffraction patterns of CNTs and Pt/CNTs. The all CNTs structures were OC-CNTs. And 1, 2,
were prepared with same conditions.

XPS analysis was performed on Pt/H-CNTs to investigate the oxidation state of Pt nanoparticles. The Pt 4f located at 71eV, C 1s at 284.14eV and O 1s located at 532.6eV, which means the successful adsorption of Pt nanoparticles with a containment of Pt oxides. The Pt(4f) peak divided into two Gaussian peaks; Pt $4f_{5/2}$ and Pt $4f_{7/2}$ which indicated at 74.28eV and 70.98eV. The difference of binding energies (ΔBE) of separated two peaks of the Pt $4f_{5/2}$ and Pt $4f_{7/2}$ is 3.33eV and an intensity ratio between these two peaks is 3:4 . The Pt $4f_{7/2}$ and Pt $4f_{5/2}$ peaks which located at 70.82eV and 74.15eV were about metallic Pt(0). The peaks of oxide Pt(II) were marked in the spectra with binding energy of 71.77eV(Pt $4f_{7/2}$) and 75.1eV(Pt $4f_{5/2}$).Finally, Pt $4f_{7/2}$ and Pt $4f_{5/2}$ were in 72.97eV and 76.3eV, which correspond to oxidized Pt(IV).

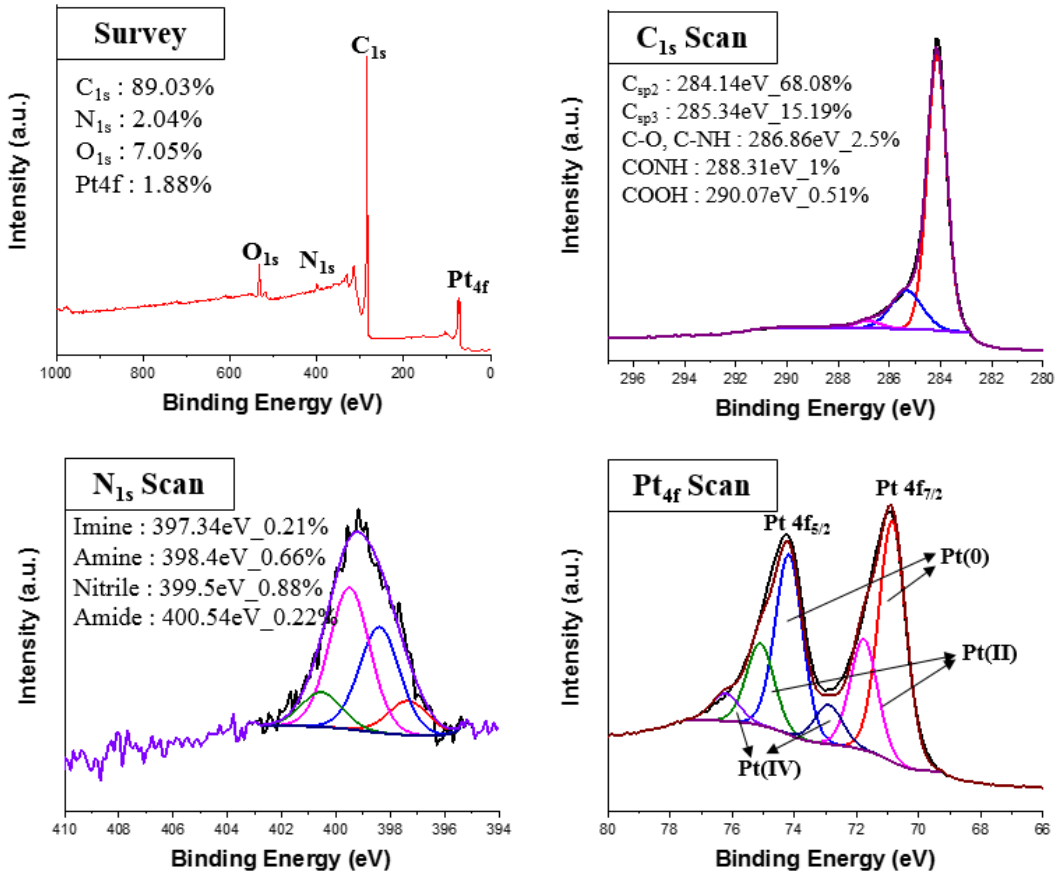

Fi_

Conclusion

We successfully carried out the adsorption of Pt nanoparticles in the range of 10-30nm diameter onto hierarchically formed CNTs grown on Si substrates and this methodology open a new approach to assemble metal nanoparticles specifically on designed surface area which can be used for further application.

List of Publications and Significant Collaborations that resulted from your AOARD supported project

a) papers published in non-peer-reviewed journals and conference proceedings

1. Hui Li, Ryi Chen, Mumtaz Ali, **Haiwon Lee*** and Min Jae Ko*, In Situ Grwon MWCNTs/MXEN Nanocomposites on Carbon Clith for High-Performanxe Flexible Supercapacitors, Adv. Funct. Mater, 2020, 30, 2002739
2. Dong-Hyeon, Rui Chen, Dengrong Sun, Jin Woo Leem, Jeong-Un Joo, Il-Suk Kang, Myung

Mo Sung, **Haiwon Lee*** and Dong-Pyo Kim*, 3D Nanoweb-like Zeolitic Imidazole Framework in a Microfluidic System for Catalytic Applications, React. Chem. Eng., 2020, 5, 1129-1134

Please notify that these two papers were supported by this project AOARD FA2386-17-1-4080. However, by unnotified PI mistake, these publications were acknowledged by the previous project AOARD FA2386-15-1-4081. Please take these two publications as cited papers.

b) conference presentations without papers - none

c) Provide a list any interactions with industry or with Air Force Research Laboratory scientists or significant collaborations that resulted from this work. - none